Hydrogen Sorption on Palladium-Doped Sepiolite-Derived Carbon Nanofibers

Chang-Keun Back,[†] Giselle Sandí,*[,‡] Jai Prakash,[†] and Jasmina Hranisavljevic[‡]

Department of Chemical and Environmental Engineering, Illinois Institute of Technology, Chicago, Illinois 60616, and Chemistry Division, Argonne National Laboratory, 9700 South Cass Avenue, Argonne, Illinois 60439

Received: March 28, 2006; In Final Form: July 5, 2006

The hydrogen sorption behavior of novel Pd-doped sepiolite-derived carbon nanofibers (SDCNs) was investigated. Two chemical doping methods of ethanol/toluene reduction and a polyol process were applied to control Pd(0) formation in the SDCNs at different Pd doping levels. Hydrogen storage capacity was observed to vary depending on the Pd particle size and doping amount as the Pd particle surface area and the carbon Brunauer−Emmett−Teller (BET) surface area change with them, suggesting the existence of an optimum Pd doping level at each doping method for the best hydrogen storage capacity. Among the samples prepared using the polyol method at different Pd amounts, the maximum hydrogen uptake of about 0.41 wt % was obtained at 298 K and 90 bar for the 5 wt % Pd-doped SDCN that has a relatively high Pd particle surface area and carbon BET surface area. Samples prepared using the ethanol/toluene reduction method exhibited a higher hydrogen uptake of about 0.59 wt % at lower Pd doping levels (3 wt % Pd) due to a smaller Pd particle size and relatively high carbon BET surface area. The hydrogen desorption behavior investigated by differential scanning calorimeter exhibited that a higher amount of hydrogen desorbed at around 860 K from the Pd-doped SDCNs compared to that from the undoped SDCN. Fourier transform infrared (FTIR) spectroscopic analysis suggested that some of the weak chemisorbed hydrogen changes to a normal covalent bond during the heating and effuses at around 860 K.

Introduction

With the increasing concerns of environmental pollution from the current use of fossil fuels and the demands for energy independence, hydrogen has been proposed as an alternative energy source, since it only produces water as products, is relatively abundant in nature, and is easily regenerated. To realize hydrogen energy systems on a large scale basis, hydrogen storage technologies have to be established because of its limitation of low energy density compared to volume. The US DOE has determined that an energy density of 6.5 wt % hydrogen and 62 kg/m^3 must be achieved in order for a hydrogen energy system with appropriate size and weight to facilitate a fuel cell vehicle driving distance of 560 km.[1] Basically, there are three hydrogen storage technologies, gas compression, liquefaction, and metal hydride, and each method shows its characteristic hydrogen storage properties depending on its strategy. Presently, however, none of the systems satisfies all the criteria with respect to storage capacity, size, cost, and safety.

Since the discovery of carbon nanotubes in 1991 by Ijiima[2] and the development of carbon nanostructures with high surface areas, hydrogen storage in carbon structures has been attracted as a new concept.[3,4] Hydrogen is physically adsorbed in carbon nanostructures through van der Waals interaction forces, and carbon structures with a high surface area are considered as candidate materials to store a large amount of hydrogen. However, in the past, some reports claiming large amounts of hydrogen stored in carbon materials were debated due to the difficulties in getting reproducible sorption amounts and the lack of theoretical explanations for their origins.[5,6] The controversies over the abilities of carbon nanostructures to store large amounts of hydrogen are mainly coming from the difficulties of precise measurements. Measured values can fluctuate depending on the test method and sample pretreatment. Also, the poor understanding of hydrogen sorption mechanisms in absorbent materials can lead to wrong conclusions. At present, with thorough theoretical approaches and careful experimental validation, it is believed that hydrogen sorption amounts are less than 1 wt % (mass weight of hydrogen per mass weight of carbon + hydrogen) at room temperature but highly increase to about 5−6 wt % at 77 K.[7,8]

Metal-doped carbon structures have been postulated as an alternative way to increase hydrogen storage capacity at room temperature due to the weak chemisorption of atomic hydrogen with higher adsorption potential than that of physisorbed hydrogen molecules.[1,9] In the system, metal nanoparticles act as catalysts to dissociate hydrogen molecules and supply atomic hydrogen to carbon active sites that are nearby. The detailed mechanism of atomic hydrogen sorption in metal-doped carbon structures is not clear yet, but it is understood that hydrogen atoms dissociated on metal catalytic sites spill over to carbon active sites and transport to the nearby carbon active sites by diffusion, prevailing atomic hydrogen sorption in the carbon structure.[10] Recent theoretical investigations using density functional theory indicated that hydrogen storage in single-wall carbon nanotubes can be increased to 7.5 wt % by saturating C−C double bonds through hydrogen chemisorption and the reaction is reversible.[11,12] Nikitin et al. experimentally proved that 5.1 wt % of hydrogen storage was obtained by hydrogenation of single-wall carbon nanotubes with atomic hydrogen using

* To whom correspondence should be addressed. Phone: (630) 252-1903. Fax: (630) 252−9288. E-mail: gsandi@anl.gov.
[†] Illinois Institute of Technology.
[‡] Argonne National Laboratory.

10.1021/jp061925p CCC: $33.50
Published on Web 07/29/2006

core-level photo electron spectroscopy and X-ray absorption spectroscopy.[13,14]

Even though there are several reports that show the enhancements in hydrogen storage capacities by doping metal catalyst in carbon structures, none of them have clearly explained the effects of metal particle size and metal doping amounts on hydrogen storage properties. In this work, the hydrogen storage capacities of Pd-doped sepiolite-derived carbon nanofibers (SDCNs) were investigated in detail at different Pd particle sizes and different Pd doping levels. To control the Pd(0) particle size, two different synthetic ethanol/toluene reduction methods and a polyol process were used. Hydrogen desorption behaviors were also investigated by using a differential scanning calorimeter and Fourier transform infrared (FTIR) spectroscopy.

Experimental Section

Synthesis and Characterization. Details about the synthesis of the carbon derived from sepiolite can be found in ref 15. The Italian sepiolite samples were obtained from Technology for Requalification and Microseparation of Materials (TRM), Viale Venezia 170, 25123 Brescia, Italy. The Spanish sepiolite was obtained from Yunclillos (Toledo, Spain), provided by TOLSA, S.A.

Ethylene or propylene was loaded and pyrolyzed in the gas phase in one step using a three-zone furnace. Quartz boats containing sepiolite were placed within a quartz tube. The temperature of the oven was gradually increased from room temperature to 700 °C. The oven was then held at the target temperature for 4 h. The clay from the loaded/pyrolyzed sepiolite sample was removed using HF, rinsed to neutral pH, and refluxed with concentrated HCl for 2 h. The sample was washed with distilled water until the pH was >5 to ensure that there was no acid left. The resultant carbon was oven-dried overnight at 120 °C. X-ray powder diffraction (XRD) patterns of sepiolite, sepiolite/organic composites, and carbons were determined using a Rigaku Miniflex, with Cu Kα radiation and a NaI detector at a scan rate of 0.5° 2Θ/min.

Transmission electron microscopy (TEM) was performed in a JEOL 400CXII transmission electron microscope operating at 100 kV. Approximately 0.01 g of the powder sample was placed into a vial containing about 10 mL of methanol. After sonicating for 30 s, copper grids with "holey" carbon films were then dipped into the resulting slurry. The Cu grids were allowed to dry for 2 h in a vacuum oven at 100 °C. Once dry, the grids were inserted into nontilt holders and loaded into the instrument. Only regions overhanging holes in the carbon grid were used. Scale markers placed on the micrographs are accurate to within 3%.

The N_2 Brunauer−Emmett−Teller (BET) surface area analysis of the resulting carbon was performed using a Micromeritics ASAP 2010 instrument. The thermal analysis was conducted with a Pyris 1 differential scanning calorimeter (DSC, Perkin-Elmer Co.) with a scanning rate of 10 °C/min. The FTIR spectra were obtained using a Spectrum GX FTIR spectrometer (Perkin-Elmer Co.)

To dope Pd on the carbon nanofibers, two synthetic methods were used. One method uses ethanol as the reducing agent. To prepare a 3 wt % Pd nanoparticle loading using this ethanol reduction method, 1.5 g of carbon nanofibers was dispersed in 20 mL of toluene and stirred for 2 h at room temperature. A 0.1 g portion of Pd(II) acetate trimer (Alfa Aesar) was added to the solution and stirred for 5 h at room temperature. After that, 2 mL of ethanol (99.0% from Aldrich) was added to the stirring solution to lead to the reduction of Pd ions on the carbon nanofibers. The solution was stirred for 10 h at room temperature. The resulting mixture was centrifuged and rinsed three times with toluene and finally vacuum-dried at 100°C overnight. The second method consisted of the polyol process. To prepare a 3 wt % Pd nanoparticle loading using this method, 1.5 g of carbon was dispersed in 8 mL of diethyleneglycol and stirred for 2 h. A 0.13 g portion of $PdCl_2$ (Alfa Aesar, 99%) was added to the solution followed by stirring at room temperature for 2 h. The temperature of the solution containing Pd(II) was increased to boiling temperature and refluxed for 2 h. The Pd-doped fibers were rinsed with diethyleneglycol and vacuum-dried at 100 °C overnight.

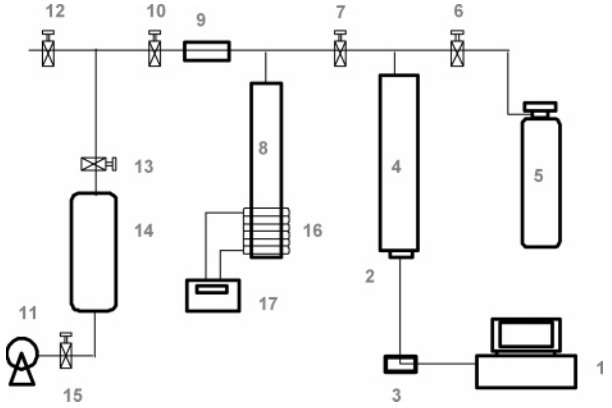

Figure 1. Schematic diagram of the hydrogen storage system: (1) PC; (2) pressure transducer; (3) multimeter; (4) hydrogen reservoir; (5) hydrogen cylinder; (6) needle valve; (7) needle valve; (8) reactor; (9) filter; (10) needle valve; (11) vacuum pump; (12) needle valve; (13) needle valve; (14) gas cylinder; (15) needle valve; (16) heating system; (17) temperature controller.

Hydrogen Adsorption/Desorption Measurements. Hydrogen sorption measurements were performed using a volumetric method. A 35 cm^3 sample holder and a 95 cm^3 hydrogen reservoir container were connected through a high pressure valve, and the pressure change as a function of time is monitored through a precision pressure sensor attached to the bottom of the hydrogen reservoir container. The schematic diagram of the equipment is shown in Figure 1. Before conducting any measurement, the equipment was tested for leaks for 24 h. Pressure and temperature calibrations were performed using an empty sample holder. A 1 g portion of sample was loaded into the sample holder and vacuum-dried at 150 °C for approximately 12 h. After cooling the sample holder to room temperature, high purity hydrogen gas (99.999%, AGA) was introduced into the sample reservoir and we waited for another 2 h until thermal equilibrium was reached. The high pressure valve between the two cylinders was slowly opened, and the hydrogen gas pressure was monitored as a function of time for 5 h. After the hydrogen sorption measurement, hydrogen was released and desorbed at 150 °C and 1×10^{-6} mbar for 5 h. The hydrogen sorption measurement was repeated for the test of reversible hydrogen sorption capacity. The number of hydrogen moles absorbed on the carbon sample was calculated using the nonideal gas equation corrected with the compressibility factor up to the second order.[16]

Results and Discussion

Parts a and b of Figure 2 show scanning electron microscopy (SEM) images of a SDCN sample consisting of disordered nanofibers whose diameter and length are of several hundred nanometers and several micrometers, respectively. The characteristic morphologies of the nanofibers are coming from the

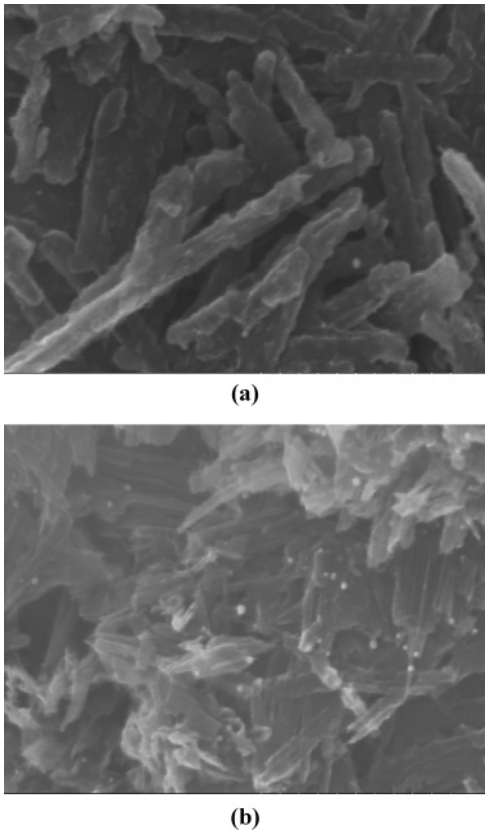

Figure 2. SEM images of Pd-nanoparticle-doped sepiolite-derived carbon nanofibers: (a) 1 wt % Pd-doped SDCN; (b) 3 wt % Pd-doped SDCN. Ethanol/toluene method used.

pyrolytic decomposition of the gaseous organic precursor (propylene) in the channels of sepiolite used as template. High resolution TEM images of the E-2 wt % Pd-doped SDCNs prepared by the ethanol/toluene reduction method are shown in Figure 3. Pd nanoparticles are seen to finely disperse on the tip or the surface of the carbon nanofibers and are in the size range of ~20 nm diameter.

X-ray diffraction (XRD) analysis on the Pd-doped SDCNs prepared by the two synthetic methods are shown in Figure 4. The peak at around 26° is the 002 reflection of graphite structure. The peaks at 40.4 and 68.1° correspond to Pd(111) and Pd-(220) reflections,[17] and the peak intensity increases as the Pd doping amount increases for both types of samples. The diffraction peaks of the Pd particles formed by the polyol process (Figure 4a) are sharp and high, indicating that the Pd particles are of a more crystalline nature and larger size than those particles formed by the ethanol reduction method. Pd(0) particle sizes were estimated by a line shape analysis using the Scherrer equation of the Pd(111) peak for the two types of Pd-doped SDCNs and shown in Figure 5. The Pd(0) particle size changes depending on the Pd doping amount and ranges from 60 to 130 nm for those particles derived by the polyol process and from 15 to 40 nm for those derived by the ethanol reduction method. For the polyol process, the Pd precursor is dissolved in diethyleneglycol which has a high dielectric constant and subsequently Pd(II) is reduced to Pd(0) in the liquid phase. The Pd metal phase is then formed and grown to Pd nanoparticles and also adsorbed to the carbon dispersed in the medium at the same time.[18] For the ethanol reduction method, the Pd(II) precursor is dissolved in toluene as the dispersion medium and adsorbed on the surface of the carbon. The adsorbed Pd(II) is subsequently reduced by the introduction of a reducing agent

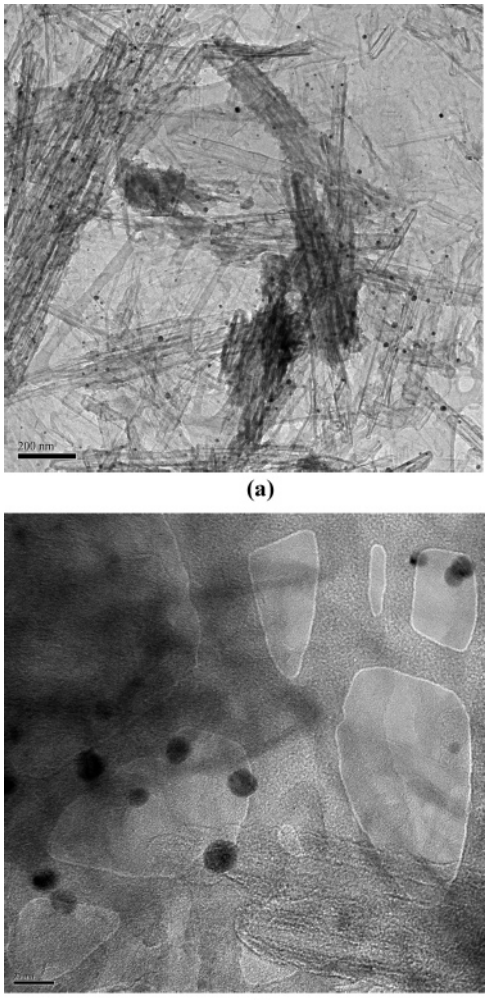

Figure 3. TEM image of a Pd-doped SDCN sample derived from the ethanol/toluene reduction method (2 wt % Pd): (a) low resolution TEM; (b) high resolution TEM.

(ethanol), thus generating smaller Pd particles on the carbon than those formed by the polyol method.[19]

Volumetrically measured hydrogen sorption isotherms of the SDCNs and the P-1 wt % Pd-doped SDCNs (prepared by the polyol process) at 298 K and 90 bar are presented in Figure 6 as a function of cycle number. There is an increase of hydrogen storage capacity by about 0.08−0.09 wt % for the P-1 wt % Pd-doped SDCNs compared to that of the undoped SDCN. Both samples show a small increase in the hydrogen storage capacity in the second cycle, which may be due to the exposure of new carbon active sites for hydrogen sorption by the removal of inert materials on the carbon surface during the first cycle of hydrogen sorption and desorption, as reported in ref 20. While the SDCN shows good reversibility of hydrogen sorption behavior after the first cycle, the P-1 wt % Pd-doped SDCN shows a slightly decreased hydrogen sorption capacity on the third cycle but levels off the remainder of the cycles. This might be the result of the strong chemisorption of some of the atomic hydrogen and not desorbed during the desorption cycle. Hydrogen sorption in Pd metal, forming metal hydride, should also be considered to understand the hydrogen sorption behaviors in the P-1 wt % Pd-doped SDCN. Pd is known to saturate with hydrogen to 0.78 (H/Pd as the atomic ratio) at 298 K and 10 MPa.[14] With the considerations of the Pd amount in the sample and the atomic ratio of 0.78 for H/Pd, about 0.01 wt % of the hydrogen sorption

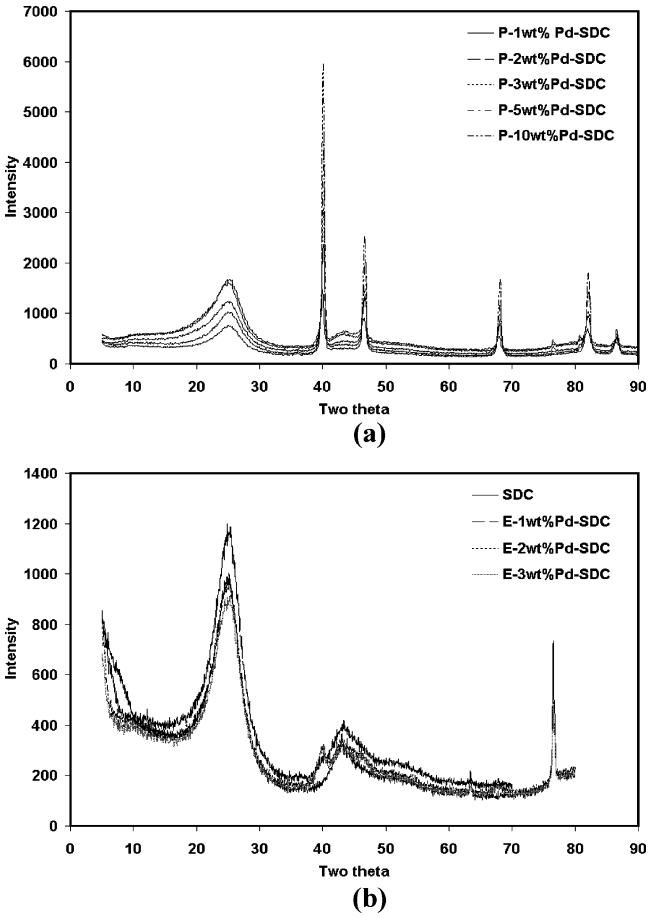

Figure 4. X-ray diffraction patterns of (a) 1, 2, 3, 5, and 10 wt % Pd-doped SDCNs prepared by the polyol process and (b) 0, 1, 2, and 3 wt % Pd-doped SDCNs prepared by the ethanol reduction method.

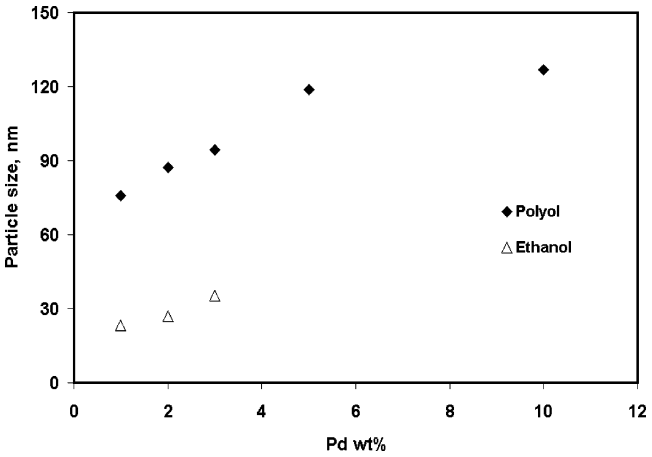

Figure 5. Pd particle sizes of the Pd-doped SDCNs prepared by the polyol process (filled diamonds) and the Pd-doped SDCNs prepared by the ethanol reduction method (empty triangles).

amount can be attributed to the formation of Pd hydride. Then, it can be known that the remaining amount of 0.07−0.08 wt % resulted by the reversible weak chemisorption of atomic hydrogen in the carbon structure, which shows the effect of Pd doping in the carbon structure for the enhancement of hydrogen storage capacity at room temperature. The enhancements in hydrogen storage capacity by metal doping in carbon structures are reported elsewhere.[9,12] Kim et al. showed about a 0.8 wt % increment of hydrogen storage capacity by doping 6 wt % Ni on MWNTs. Yoo et al. reported a 0.7 wt % increment by doping

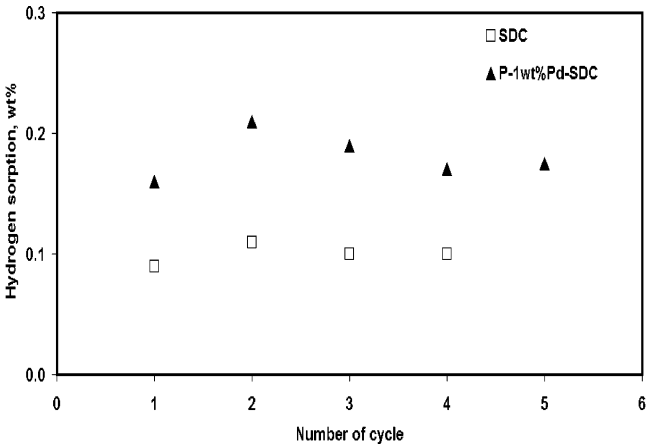

Figure 6. Hydrogen storage amounts as a function of cycle number for the SDC (empty squares) and 1 wt % Pd-doped SDC by the polyol process (filled triangles) at 298 K and 90 bar.

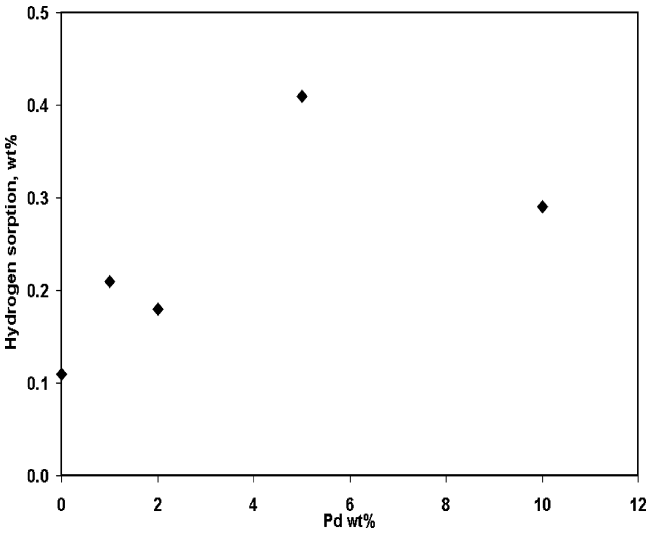

Figure 7. Hydrogen storage amounts at 298 K and 90 bar of 0, 1, 2, 5, and 10 wt % Pd-doped SDCNs prepared by the polyol process.

Pd and oxidizing carbon nanotubes with La and claimed the importance of carbon active sites created by dangling bonds and defective sites for higher hydrogen sorption amounts.

Figure 7 shows the hydrogen sorption isotherms at 298 K and 90 bar for various amounts of Pd-doped SDCNs prepared by the polyol process. Unlike the claims reported in ref 14 showing good correlation between hydrogen storage capacity and Pd/C ratio, in our system, the hydrogen storage capacity was observed to vary depending on the Pd doping amount. Among the samples, the maximum hydrogen storage capacity of about 0.41 wt % was obtained for the P-5 wt % Pd-doped SDCN. The hydrogen storage capacity is about 4 times larger than that of the undoped SDCN. The P-10 wt % Pd-doped SDCN shows small hydrogen storage capacity even though it contains the highest amount of Pd. Figure 8 shows the change of the carbon BET surface area with the Pd doping amount. The change of the carbon BET surface area is considered to be a result of the blocking or filling of carbon micropores with Pd particles, which means that the Pd particle size and amount are controlling factors to determine the carbon BET surface area at a given carbon pore size. On the basis of the assumptions that the hydrogen molecule is dissociated on the surface of the Pd particle and atomic hydrogen diffuses and adsorbs on carbon active sites, the Pd particle surface area and carbon surface area

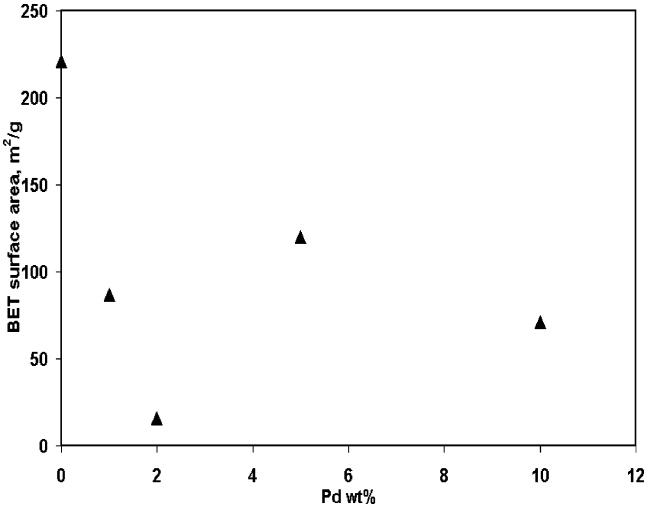

Figure 8. BET specific surface areas of 0, 1, 2, 5, and 10 wt % Pd-doped SDCNs prepared by the polyol process.

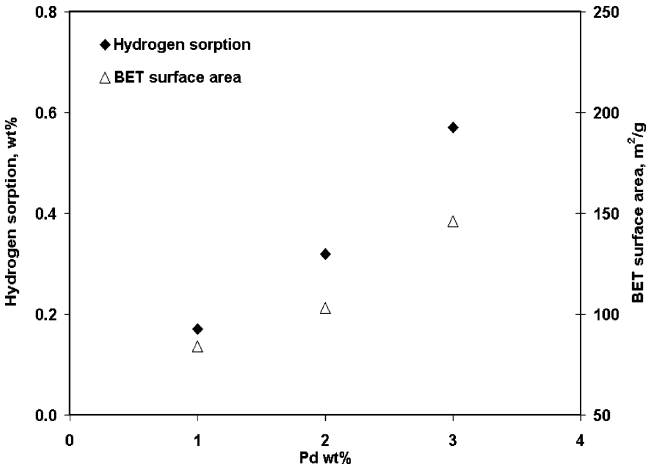

Figure 9. Hydrogen storage amount (filled diamonds) and BET specific surface area (empty triangle) of 1, 2, and 3 wt % Pd-doped SDCNs prepared by the ethanol reduction method.

are important factors that have an influence on the hydrogen storage capacity of the Pd-doped carbon structure. On the basis of these considerations, the low hydrogen storage capacity observed on the 10 wt % Pd-doped SDCN might be due to the large Pd particle size and the low carbon BET surface area. Figure 9 shows the hydrogen sorption isotherms at 298 K and 90 bar and the BET specific surface areas for the Pd-doped SDCNs prepared by the ethanol/toluene reduction method as a function of Pd doping amount. The BET specific surface area increases with Pd doping amount unlike that observed on the samples by the polyol process. The different trend of carbon BET specific surface area with Pd doping is due to the much smaller Pd particle size. The hydrogen storage capacity increase with the Pd doping amount and the highest hydrogen uptake was observed on the E-3 wt % Pd-doped SDCN for about 0.59 wt %, which is about 50% higher than that of the P-5 wt % Pd-doped SDCN. The schematic studies of the hydrogen storage capacity and carbon BET specific surface area in the higher Pd doping levels are under study. Recently, Yang et al.[21,22] reported that a carbon bridge connecting a metal particle and a carbon receptor (SWNT, AX-21, for example) is important in hydrogen sorption of metal-doped carbon structures. The group claimed that a carbon bridge creates a more intimate contact between a metal particle and a receptor and a hydrogen molecule dissociated by a metal particle spills over the carbon bridge and diffuses to the carbon active sites of the receptor. The effect of a carbon bridge is of interest to our system and will be addressed in the future work for more enhanced hydrogen storage capacity.

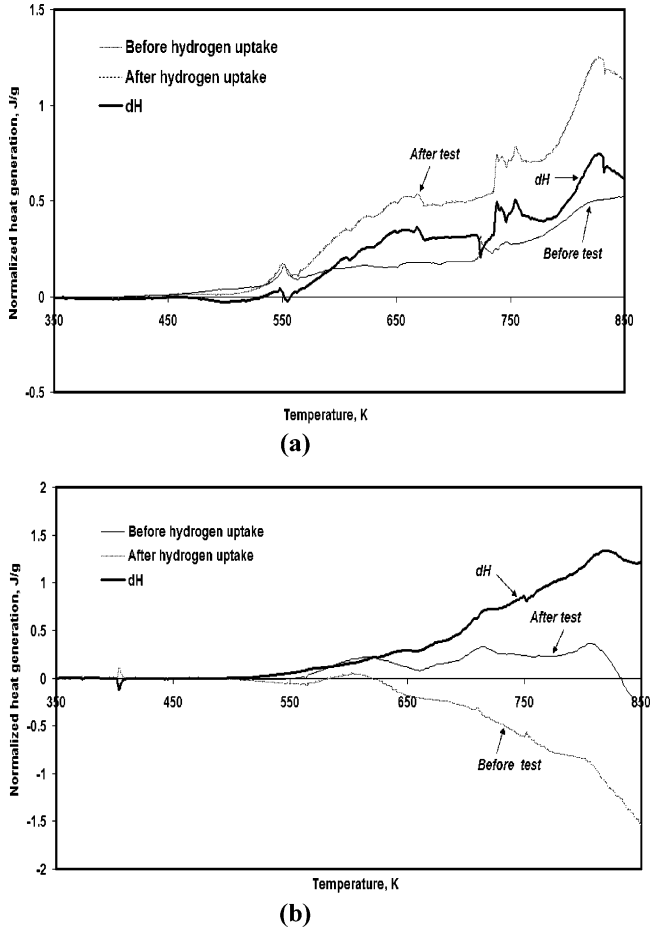

Figure 10. DSC analysis of (a) undoped SDCN and (b) 3 wt % Pd-doped SDCN prepared by the ethanol reduction method before and after hydrogen uptake.

The investigations on the hydrogen desorption behaviors of the Pd-doped SDCNs were performed using a DSC. For comparison, the undoped SDCN was also tested. The undoped SDCN and the E-3 wt % Pd-doped SDCN were tested before and after hydrogen uptake, and the heat evolutions involved with the hydrogen desorption could be obtained by subtracting the DSC data before hydrogen uptake from them after hydrogen uptake. The DSC analyses are presented in parts a and b of Figure 10 for the undoped SDCN and the E-3 wt % Pd-doped SDCN, respectively. The heat generations are seen to initiate from about 520 K for both samples. Two small peaks are observed at around 550 K for the samples, especially for the undoped SDCN. The peaks are not known yet because the desorption temperature even for strongly physisorbed hydrogen is much lower than the temperature, as reported in ref 23. In the higher temperature range, roughly three different desorption peaks are seen at about 650, 720, and 830 K for the both samples. From refs 24 and 25, the peak at around 650 K is due to the hydrogen desorption from carbon defective sites and dangling bonds, while the peak at around 830 K evolves by the hydrogen desorption from the covalent bonds between C−H. The peak observed at 720 K is not clear and still under investigation. The comparison between the subtracted DSC data for the undoped SDCN and the E-3 wt % Pd-doped SDCN exhibits that the latter sample generated a higher amount of

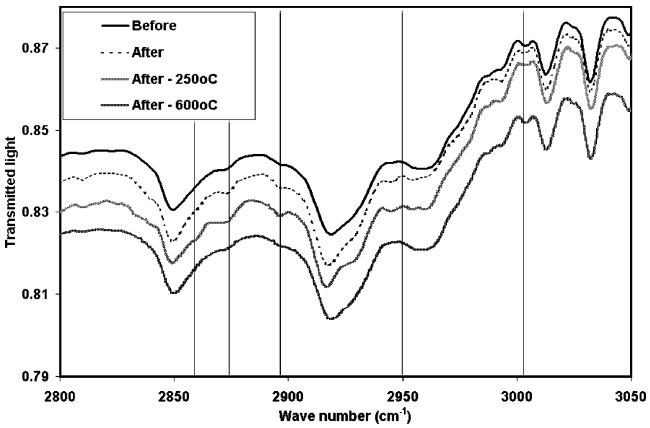

Figure 11. FTIR spectroscopic analyses on the E-3 wt % Pd-doped SDCN before and after hydrogen uptake at room temperature.

TABLE 1: Various C−H Stretching Vibration Bands

configuration	predicted frequency (cm^{-1})
sp^1CH	3305
sp^2CH (arom)	3050
sp^2CH_2(olef)	3020
sp^2CH (olef)	3000
sp^3CH_3 (asym)	2960
sp^2CH_2 (olef)	2950
sp^3CH_2 (asym)	2925
sp^3CH	2915
sp^3CH_3 (sym)	2870
sp^3CH_2 (sym)	2855

hydrogen at around 830 K, which clearly proves the enhanced hydrogen sorption property of the Pd-doped SDCN. The desorption temperature, however, indicates that the increased amount of hydrogen was mostly stored by covalent bonding to carbon in the Pd-doped SDCN, which was not intended in this work, since weak reversible chemisorption of atomic hydrogen was expected with lower desorption temperature, as reported in ref 9.

FTIR spectroscopic analyses on the E-3 wt % Pd-doped SDCN before and after hydrogen uptake at room temperature were performed to see whether atomic hydrogen is covalently bonded to carbon during the hydrogen sorption cycle. In addition, the sample was heated to 600 °C and spectroscopically analyzed to see the change of the C−H bond. The FTIR spectroscopic results are presented in Figure 11, and the corresponding peaks are listed in Table 1. After the hydrogen uptake, the peaks for sp^3 C−H stretching at 2870 and 2925 cm^{-1} are observed to increase their intensity, which means that some of the atomic hydrogen is covalently bonded to carbon. Upon heating to about 250 °C, the peaks for sp^3 C−H stretching grow more and then decrease upon heating to 600 °C. The similar but opposite trend for sp^2 C−H stretching at 3002 cm^{-1} is also observed. Koidl et al.[27] reported that weakly bonded hydrogen is thermally converted into normally bonded hydrogen upon thermal annealing at 300 °C, resulting in the change of sp^2 to sp^3, but after heating to 600 °C, hydrogen effuses and sp^3 changes to sp^2. Their results are consistent with our results. From the FTIR spectroscopic analyses on the Pd-doped SDCNs after hydrogen uptake and upon heating to 600 °C, it can be explained that some of the atomic hydrogen is covalently bonded to carbon during the hydrogen sorption cycle at room temperature and also some of the weakly chemisorbed hydrogen can change to a normal bond during the heating to about 250 °C, as observed with the peak growing for the sp^3 C−H stretching, and the covalently bonded hydrogen effuses upon heating to around 600 °C. The FTIR spectroscopic analyses provide an understanding as to why the Pd-doped SDCNs generated the higher hydrogen desorption at around 830 K. The exact and detailed mechanisms for hydrogen desorption from the Pd-doped SDCNs are still under study.

Conclusions

The characteristic hydrogen storage properties of the Pd-doped SDCNs have been investigated with the considerations of Pd particle size and Pd doping amount. Enhanced hydrogen storage capacity was observed by doping Pd in the SDCN, and the enhancement of hydrogen storage capacity was varied depending on the Pd particle size and Pd doping amount. Among the samples prepared by the polyol process, the maximum hydrogen storage capacity of about 0.41 wt %, about 4 times larger than that of the un-doped SDCN, was seen on the P-5 wt % Pd-doped SDCN having a relatively high Pd particle surface area and high carbon BET surface area. The effect of smaller size Pd doping on hydrogen storage capacity was seen with the hydrogen sorption measurements on the samples prepared by the ethanol/toluene reduction method. The higher hydrogen storage capacity of 0.59 wt % was seen on the E-3 wt % Pd-doped SDCN even though smaller amount of Pd was contained in the sample compared to the P-5 wt % Pd-doped SDCN. The investigations on the hydrogen desorption behaviors of the Pd-doped SDCN with DSC and FTIR showed that some of the atomic hydrogen can be covalently bonded to carbon during the hydrogen sorption cycle but weakly chemisorbed atomic hydrogen also changed to a normal bond upon heating to about 250 °C and desorbs at a high temperature of about 600 °C.

Acknowledgment. This work was performed under the auspices of the Office of Basic Energy Sciences, Division of Chemical Sciences, Geosciences, and Biosciences, U.S. Department of Energy, under Contract No. W-31-109-ENG-38.

References and Notes

(1) DOE hydrogen program, FY 2004 Progress Report.
(2) Iijima, S. *Nature* **1991**, *354*, 56.
(3) Zhao, X. B.; Xiao, B; Fletcher, A. J.; Thomas, K. M. *J. Phys. Chem. B* **2005**, *109*, 8880.
(4) Shiraishi, M.; Takenobu, T.; Ata, M. *Chem. Phys. Lett.* **2003**, *367*, 633−636.
(5) Dillon, A. C.; Jones, K. M.; Bekkedahl, T. A.; Kiang, C. H.; Bethune, D. S.; Heben, M. J. *Nature* **1997**, *386*, 377.
(6) Dillan, A. C.; Gennet, T.; Alleman, J. L.; Jones, K. M.; Parilla, P. A.; Heben, M. J. Proceeding of the 2000 hydrogen program review, May 8−10, 2000, NREL/CP-570−28890, 2000.
(7) Ye, Y.; Ahn, C. C.; Witham, C.; Fultz, B. *Appl. Phys. Lett.* **1999**, *74* (16), 19.
(8) Shiraishi, M.; Takenobu, T.; Kataura, H.; Ata, M. *Appl. Phys. A* **2004**, *78*, 947.
(9) Kim, H. S.; Lee, H.; Han, K. S.; Kim, J. H.; Song, M. S.; Park, M. S.; Lee, J. Y.; Kang, J. K. *J. Phys. Chem. B* **2005**, *109*, 8983.
(10) Conner, W. C., Jr.; Falconer, J. L. *Chem. Rev.* **1995**, *95*, 759.
(11) Park, S.; Srivastava, D.; Cho, K. J. *Nano Lett.* **2003**, *3*, 1273.
(12) Yoo, E.; Gao, L.; Komatsu, T.; Yagai, N.; Arai, K.; Yamazaki, T.; Matsuishi, K.; Matsumoto, T.; Nakamura, J. *J. Phys. Chem. B* **2004**, *108*, 18903.
(13) Nikitin, A.; Ogasawara, H.; Mann, D.; Denecke, R.; Zhang, Z.; Dai, H.; Cho, K.; Nilsson, A. *Phys. Rev. Lett.* **2005**, *25*, 225507.
(14) Lupu, D.; Biris, A. R.; Misan, I.; Jianu, A.; Holzhuter, G.; Burkel, E. *Int. J. Hydrogen Energy* **2004**, *29*, 97.
(15) Sandí, G.; Winans, R. E.; Carrado-Gregar, K. U.S. Patent 6,110,-621.
(16) Smith, J. M. *Introduction to Chemical Engineering Thermodynamics*; McGraw-Hill: 2001.
(17) Xue, B.; Chen, P.; Hong, Q.; Lin, J.; Tan, K. L. *J. Mater. Chem.* **2001**, *11*, 2378.

(18) Fievet, F.; Lagier, J. P.; Figlarz, M. *MRS Bull.* **1989**, 29.
(19) Dekany, I.; Turi, L.; Szucs, A.; Kiraly, Z. *Colloids Surf., A* **1998**, *141*, 405.
(20) Park, C.; Anderson, P. E.; Chambers, A.; Tan, C. D.; Hidalgo, R.; Rodriguez, N. M. *J. Phys. Chem. B* **1999**, *103*, 10572.
(21) Lachawiec, A. J.; Qi, G.; Yang, R. T. *Langmuir* **2005**, *21*, 11418.
(22) Yang, F. H.; Lachawiec, A. J.; Yang, R. T. *J. Phys. Chem. B* **2006**, *110*, 6236.
(23) Han, S. S.; Kim, H. S.; Han, K. S.; Lee, J. Y.; Lee, H. M.; Kang, J. K. *Appl. Phys. Lett.* **2005**, *87*, 213113.
(24) Fujji, H.; Orimo, S. I. *Physica B* **2003**, *328*, 77.
(25) Fukunaga, T.; Itoh, K.; Orimo, S.; Aoki, M.; Fujii, H. *J. Alloys Compd.* **2001**, *327*, 224.
(26) *Handbook of Chemistry and Physics*, 8th ed.; CRC: 2005−2006.
(27) Dischler, B.; Bubenzer, A.; Koidl, P. *Solid State Commun.* **1983**, *48*, 105.